NeuroImage 51 (2010) 1098–1105

Contents lists available at ScienceDirect

NeuroImage

journal homepage: www.elsevier.com/locate/ynimg

The contributions of myelin and axonal caliber to transverse relaxation time in shiverer and neurofilament-deficient mouse models

Victor V. Dyakin [a,b], Yuanxin Chen [a,b], Craig A. Branch [b,c,d], Veeranna [a], Aidong Yuan [a,e], Mala Rao [a,e], Asok Kumar [a], Corrinne M. Peterhoff [a], Ralph. A Nixon [a,e,f,*]

[a] Center for Dementia Research, Nathan Kline Institute Orangeburg, New York, USA
[b] Center for Advanced Brain Imaging, Nathan Kline Institute Orangeburg, New York, USA
[c] Department of Radiology, Albert Einstein College of Medicine, Bronx, New York, USA
[d] Departments of Radiology and Physiology and Biophysics, Albert Einstein College of Medicine, Bronx, New York, USA
[e] Department of Psychiatry, New York University School of Medicine, New York, USA
[f] Department of Cell Biology, New York University School of Medicine, New York, USA

ARTICLE INFO

Article history:
Received 24 August 2009
Revised 1 March 2010
Accepted 3 March 2010
Available online 11 March 2010

Keywords:
T2 relaxation
Iron
White matter
Neurofilament
Microtubules
Myelin
Shiverer mice

ABSTRACT

White matter disorders can involve injury to myelin or axons but the respective contribution of each to clinical course is difficult to evaluate non-invasively. Here, to develop a paradigm for further investigations of axonal pathology by MRI, we compared two genetic mouse models exhibiting relatively selective axonal or myelin deficits using quantitative MRI relaxography of the transverse relaxation times (T2) *in vivo* and ultrastructural morphometry. In HM-DKO mice, which lack genes encoding the heavy (NF-H) and medium (NF-M) subunits of neurofilaments, neurofilament content of large myelinated axons of the central nervous system (CNS) is markedly reduced in the absence of changes in myelin thickness and volume. In shiverer mutant mice, which lack functional myelin basic protein, CNS myelin sheath formation is markedly reduced but neurofilament content is normal. We observed increases in T2 in nearly all white matter in shiverer mice compared to their wild type, while more subtle increases in T2 were observed in HM-DKO in the corpus callosum. White matter T2 was generally greater in shiverer mice than HM-DKO mice. Ultrastructural morphometry of the corpus callosum, which exhibited the greatest T2 differences, confirmed that total cross-sectional area occupied by axons was similar in the two mouse models and that the major ultrastructural differences, determined by morphometry, were an absence of myelin and larger unmyelinated axons in shiverer mice and absence of neurofilaments in HM-DKO mice. Our findings indicate that T2 is strongly influenced by myelination state and axonal volume, while neurofilament structure within the intra-axonal compartment has a lesser effect upon single compartment T2 estimates.

Introduction

Structural and functional changes in white matter (WM) regions of the brain are often seen in other brain disorders, including traumatic brain injury (Yuan et al., 2007), certain metabolic disorders (Kaye, 2001), multiple sclerosis (MS) (Pascual-Lozano et al., 2007) and neuropsychiatric disorders, including dementia, schizophrenia, depression and bipolar disorder (Brant-Zawadzki et al., 1985; Cheung et al., 2008; Figiel et al., 1991). Injury to either the axonal cytoskeleton or to myelin can cause neuronal dysfunction leading to significant long-term clinical disability (Kerschensteiner et al., 2004), although assessing the relative contribution of each type of injury to clinical outcomes is difficult. In MS, for example, clinical imaging often focuses upon determination of vascular permeability and preservation of axons, while increasing evidence (Song et al., 2002; Trapp et al., 1999) indicates that axonal degeneration within long myelinated fiber tracts may be an important determinant of permanent clinical deficits. Specific imaging measures of myelin integrity, however are not currently available, although diffusion tensor imaging (DTI) (Kolind et al., 2008; Song et al., 2002), magnetization transfer contrast (Giacomini et al., 2009; McCreary et al., 2009) and multi-compartmental transverse relaxivity (T2) measurements (Laule et al., 2008; Whittall et al., 1997) hold promise as specific measures of axonal myelin constitution or demyelination and remyelination processes.

In diseases involving white matter, T2 enhancement is common but the specific nature of the mechanism underlying the T2 change remains controversial (Valk and Barkhof, 2005). Increased vascular permeability can lead to increased extracellular water (edema) while cellular swelling may attenuate T2. Conversely, subtle loss of myelin may lead to a more hydrophilic environment, possibly attracting water and shifting the compartmentalization of water within the tissue. This type of myelin pathology may be visible as a subtle T2

* Corresponding author. Center for Dementia Research, Nathan Kline Institute, 140 Old Orangeburg Road, Orangeburg, NY 10962, USA. Fax: +1 845 398 5422.
E-mail address: nixon@nki.rfmh.org (R.A. Nixon).

1053-8119/$ – see front matter © 2010 Elsevier Inc. All rights reserved.
doi:10.1016/j.neuroimage.2010.03.013

enhancement by magnetization transfer contrast (McCreary et al., 2009; Ou et al., 2009; Zaaraoui et al., 2008) or a re-compartmentalization of the tissue water. Sensitive and robust methods for the multi-compartmental assessment of T2 rates and weights in white matter are thus needed to characterize white matter pathology associated with myelination state.

Advances in quantitative MRI and improved image-processing tools have enabled the mapping of neuroanatomical and neuropathological abnormalities in small animals, especially at high magnetic fields. Correlation of T2 relaxation with properties of the myelin sheath has been previously reported (Degaonkar et al., 2005; Ford et al., 1990; McArdle et al., 1987) but without assessment of WM morphology leaving unresolved the question of whether white matter T2 is mainly dependent on the cytoskeletal or myelination state. In the present study we have contrasted T2 relaxation times in two mouse models exhibiting selective myelin or axonal deficits, respectively. The shiverer (Shi) mouse expresses an autosomal recessive mutation of the myelin basic protein (MBP) gene that results in markedly reduced MBP levels and incomplete CNS myelin sheath formation, leading to axon conduction deficits progressive tremor and ataxia, seizures, and shortened life-span (Martin et al., 2006; Rosenbluth, 1980; Seiwa et al., 2002; Shen et al., 1985). The absence of evident axonal injury or inflammatory reactions (Griffiths et al., 1998) makes the Shi mouse a suitable model for MRI investigations of primary dysmyelination without confounding axonal degeneration. For comparison, we also examined the HM-DKO mouse, a genetically engineered model lacking the heavy and middle neurofilament subunits leading to a profound and selective deficit of axonal neurofilaments. We believed that this model, in combination with the shiverer mouse, would provide an opportunity to discriminate between intra-axonal deficits and primary myelin deficits upon the T2. Furthermore, by examining the ultrastructural morphometry of both models, we aimed to provide a suitable paradigm for future investigations of relationships between ultrastructural axonal pathology and *in vivo* T2 relaxation or other imaging parameters relevant to white matter analysis.

Materials and methods

Mouse models

Shiverer arose as a spontaneous mutation (Rosenbluth, 1980) and is maintained on a C3HeB/FeJ background. HM-DKO double knockout mice, maintained on a C57B1/6 background, were generated by cross breeding NF-M knockout mice, generously provided by Dr. Jean-Pierre Julien (Quebec, Canada) with our NF-H knockout mice. CNS neurofilaments are linear polymers composed of four subunits, including the 64 kDa α-internexin; and the light (NF-L), mid-sized (NF-M), and heavy (NF-H) NF subunits, with respective molecular masses SDS-PAGE gels of ~70, 150, and 200 kDa (Yuan et al., 2006). By forming a network in axons, neurofilaments add tensile strength to axons and dendrites and maintain the large calibers of axons by filling space. Loss of neurofilament content reduces axonal caliber leading to hind-limb paralysis in later life (Elder et al., 1999; Jacomy et al., 1999).

MRI protocols

10 Shi mice (mean 4.0 months, standard deviation [sd] 0.25 months), 6 HM-DKO mice (mean 5.0 months, sd 0.50 months), and 16 littermate WT controls [10 WT(Shi) (mean 4.0 months, sd 0.25 months), and 6 WT(HM-DKO)] (mean 4.8 months, sd 0.25 months). MRI was performed at 7 T (Magnex Scientific, Oxford, UK) on an SMIS spectrometer (Surrey Medical Imaging systems, Guilford, UK). Animals were induced with isoflurane (2.0%) in NO2 (76%) and O2 (22%). After successful induction, the animals were transferred to an MR safe holder utilizing head restraints and isoflurane was reduced to 1%. Rectal temperature was maintained at 37 °C ± 0.5 °C during imaging with a warm water pad, and respiration rate was monitored continuously using an S.A.R. monitor (Bayshore, NY). T2 weighted images were acquired using a 45 mm ID homogeneous 8 rod birdcage coil and a multi-slice single-echo sequence (Guilfoyle et al., 2003) with 2 averages and phase alternation which employed apodized 5 cycle sinc pulses for excitation and refocusing. These methods have been previously reported (Chen et al., 2009; Falangola et al., 2005; Falangola et al., 2007) and were employed because they provided robust estimates of single compartment relaxation over the entire brain in a long but acceptable length of time. Our studies have typically employed single compartment estimates, as we have found them reliable means to characterize pathological differences between wild type and transgenic animals. T2 relaxometry was achieved by varying the echo time (TE = 15, 20, 25, 35, 55, and 75 ms) of the sequence with constant repetition time (TR = 4000 ms). Forty-eight 0.2 mm thick slices were acquired (with gap = 0.1 mm) on a 128*128 matrix over a field of view (FOV) of 25.6 mm, yielding voxels $0.2 \times 0.2 \times 0.2$ mm^3. The total MR scanning time, including calibration, was about 128 min for each animal. Images were reconstructed using Hanning filters and all images were reconstructed using preset scaling from the image with the shortest echo time. Absolute T2 maps were calculated on a voxel-by-voxel basis as described below. Because of the high-resolution and excellent contrast available, the shortest echo time image was employed for quantitative morphological analyses.

Image analysis

Images were converted to analyze format and read into the MEDX image-processing package (Medical Numerics, Inc, Germantown, Maryland). After brain masking, the T2 relaxation time was estimated from each voxel time series within each brain using a two parameter, single compartment fit (M0 and T2) via linear regression on the log-linear data. For evaluation of T2 fitting quality "Sum of Squares" map (MEDEX) was generated. In addition, ROI fitting quality was estimated (Excel). This produced a T2 map for each of the 48 slices of each animal. Regions of interest (ROIs) were manually drawn on the high-resolution T2-weighted images of each mouse in the MEDx software package.

Anatomical guidelines for outlining these regions were determined by comparing anatomical structures in the MRI slices with a standard atlas (Franklin and Paxinos, 1997). Regions analyzed include cortex (bregma 1.70 to −4.72 mm), hippocampus (−0.94 to −4.16 mm), corpus callosum (1.70 to −4.72 mm), anterior commissure, (1.18 to 0.26 mm), thalamus (−0.94 to −4.0 mm), and cerebellum (−5.88 to 8.12 mm). For each animal, a fixed number of slices with equivalent anatomy were selected to achieve a comparable measure between animals. The mean T2 within a region of interest (ROI) was estimated by averaging the T2s from each voxel contained within the ROI to yield an average T2 for that animal ROI. T2 values were then averaged across animals to provide the group T2 with standard deviation of the mean. Volumes of each structure were estimated by multiplying the number of pixels within an ROI by the size of each voxel and the slice thickness in high-resolution T2-weighted images. One-way analysis of variance (ANOVA) was performed to assess the between-group variance, followed by a between-group analysis of the mean T2 values and anatomical volumes using the Student's paired *t*-test or Welch's *t*-test where appropriate.

Immunohistochemistry

A subset of the 16 mice used for imaging (HM-DKO mice, 4 males, 4 months and 12 days old; WT mice, 4 males, 4 months and 7 days old; Shi mice, 4 males, 4 months and 14 days old, and WT(Shi) mice, 4 males, 4 months and 3 days old) was selected for immunohistochemical

analysis. Mice were deeply anesthetized with sodium pentobarbital (60 mg/kg) and perfused transcardially with 4% paraformaldehyde (PFA) in 0.1 M phosphate buffer, pH 7.4, delivered with a peristaltic pump at 20 ml/min for 5 min. Brains were removed and post-fixed overnight in the same fixative at 4 °C. 40 μm sections were cut with a vibratome (Leica, Nussloch, Germany) and then kept at 4 °C in Tris-buffered saline (TBS; pH 7.5). Antibodies to demonstrate the presence of neurofilament subunits were used as follows: monoclonal b-cyto 13 (1:10), a phosphorylation independent antibody that recognizes NF-H, -M and -L [generated at NKI (Rao et al., 2008)]; monoclonal SMI-33 (1:100), specific to a non-phosphorylated epitope accessible in both phosphorylated and non-phosphorylated NF-H and -M (Covance, Princeton, NJ); polyclonal antibody 15-2 (1:500), generated against NF-L [generated at NKI (Veeranna et al., 2004)]; monoclonal α-internexin (1:200; clone 2E3; Millipore, Temecula, CA) and SMI99, directed against myelin basic protein (1:100; Covance, Princeton, NJ). Immunocytochemistry employed standard procedures. Briefly, free-floating tissue sections were rinsed in TBS, and incubated for 30 min in 3% H2O2. The sections were incubated for 1 h in blocking reagent (Vector Laboratories; Burlingame, CA), followed by incubation with the primary antibody for 24 h at 4 °C. Sections were incubated for 30 min in the appropriate biotinylated secondary antibody (Vector Laboratories; Burlingame, CA), processed using the ABC solution (Vector Laboratories) and visualized with 3,3′-diaminobenzidine (DAB; Vector Laboratories). Tissue incubated in the absence of primary and secondary antibodies was processed simultaneously as a negative control. Sections were examined on a Zeiss Axioskop II equipped with an AxioCam HrC digital camera operated through AxioVision 4.6 software. Following Kohler alignment, white balance was equalized to ensure even illumination of the field. Auto-exposure was used and all fields were captured using the same exposure time.

Western blot analysis of CC

Corpus callosa from each of four Shi, HM-DKO and corresponding WT mice were surgically removed from the brain, frozen on dry ice and stored at −80 °C. Frozen tissues were homogenized on ice in a buffer containing 50 mM Tris (pH 7.5), 0.5 mM EDTA (pH 8), and 1 mM each of PMSF, aprotinin, pepstatin, 20 mM beta glycerol-phosphate, 10 mM sodium fluoride and 1 mM sodium orthovanadate. An equal volume of a solution containing 50 mM Tris (pH 7.5), 150 mM NaCl, 1% NP-40, 1% sodium deoxycholate, and 2% SDS was added and homogenates were sonicated for 20 s, boiled for 10 min and clarified by centrifugation at 16,000×*g* for 5 min in a table top cold centrifuge. Protein determination was carried out using the bicinchoninic acid (BCA) protein assay kit (Pierce Chemical Co.; Rockford, IL). Protein extracts together with dual color prestained protein molecular weight standards (Biorad) were separated by SDS-PAGE using gels containing 7.5% polyacrylamide. The gels were then electroblotted onto nitrocellulose membranes. Immunodetection of the protein of interest was performed by blocking the membrane in 3% nonfat dry milk in PBST (PBS, 0.02% Tween 20) for 1 h followed by washing in PBST thrice to remove the milk. The membranes were then incubated overnight with specific primary antibody diluted in TBST containing 0.5% BSA and 0.02% sodium azide. Antibodies (and dilutions) were used as follows: monoclonal antibodies SMI31 (1:1000), reactive with a phosphorylated epitope in heavily phosphorylated NF-H and -M; , SMI 33 (1:2000), described above; SMI-99 (1:5000) directed against MBP (all from Covance; Princeton, NJ); RMO-44 (1:2000), against NF-M (Invitrogen; Carlsbad, CA); NR-4 (1:1000) against NF-L (Sigma; St. Louis, MO) and α-internexin (1:300; Millipore). The membranes were developed using enhanced chemiluminescence kit (Amersham) and exposed to X-ray films. The bands of interest were determined by the apparent molecular weight of the target protein. Films were scanned using an HP ScanJet 4070 Photosmart scanner. Images were saved in .tiff file format and processed using Adobe Photoshop and the optical densities (OD) of the appropriate bands were quantified on a Macintosh computer using the public domain NIH Image program (version 6.1), developed at the U.S. National Institutes of Health and available on the Internet at http://rsb.info.nih.gov/nih-image. Band intensities were calculated by subtracting the background OD value from the measured OD of each immunolabeled band.

Electron microscopy (EM) and morphometry

Mice [$n=4$ for each group of WT(HM-DKO), HM-DKO, WT(Shi) and Shi mice], at the same ages as were used for immunocytochemistry were anesthetized and fixed by vascular perfusion with a solution containing 4% paraformaldehyde, 1% glutaraldehyde, 0.1 M sodium cacodylate buffer, at pH 7.2. After the brains were dissected out, 50 μm sections were cut, post-fixed for 1 h with 1% osmium tetroxide, dehydrated in a graded ethanol series, and embedded in Epon. Sections of 1 μm were stained with toluidine blue (JBS; Dorval, CA) and examined by light microscopy. Subsequent ultra-thin sections were collected on copper grids, stained with uranyl acetate and lead citrate and examined in a transmission EM. Representative fields from the corpus callosum from each genotype were collected at 25,000× and used for morphometric analyses. The total numbers of axons counted in each group were: 910 (HM-DKO), 1026 (Shi), 922 [WT(HM-DKO)], and 930 [WT(Shi)]. Using Bioquant software (R&M Biometrics, Inc., Nashville, TN), the areas occupied by myelin (surrounding myelinated axons) and by axoplasm, in myelinated and unmyelinated axons were visually inspected and manually traced and measured. Cross-sectional areas for myelin [*S*(M)], axoplasm of myelinated axons [*S*(my)], and unmyelinated axons [*S*(un)] were calculated by summing the total areas of each in a 12.645 m^2 field. The remaining area within each micrograph, termed *S*(rest), was composed mostly of glial processes, and was calculated by subtracting the sums of *S*(M), *S*(my) and *S*(un) from the total area.

Results

MRI volumetric analysis of HM-DKO and Shi mice

Volumetric measurements were made from the high-resolution T2-weighted images collected from each group of animals. Brain regions with clearly definable anatomic boundaries were determined from coronal slices collected from multi-slice data sets. Areas measured include cingulate cortex (CT), hippocampus (HP), CC, cerebellum (CB), anterior commissure (AC), striatum (ST) and thalamus (TM). Whole brain (WB) volumetric measurements did not differ between the WT (Shi) and the WT (HM-DKO) mice (ANOVA, $p>0.05$). Subsequently, WB volume was significantly reduced in the HM-DKO mice (10%, $p<0.01$), but not significantly reduced in Shi mice ($p=0.054$) when compared to their corresponding WT controls (Fig. 1A). Regional comparisons revealed disproportionately greater loss of volume in the CC than in other brain regions in both HM-DKO mice (32%, $p<0.001$) and Shi mice (22%, $p<0.05$) when compared to their WT controls (Fig. 1B).

Differences in T2 between WT, HM-DKO and Shi mice

Examples of the T2 maps of representative animals from each the four groups are presented in Fig. 2 (A–D) along with representative maps of the squared errors from each T2 map (E–H). Drawn on each T2 map is, for the representative slice, the ROI used to define the corpus callosum for T2 measurements in that tissue. As can be seen from the T2 maps, there is a diminished contrast within the shiverer map, compared to the other maps, while the variability in the squared errors was least in the shiverer map. Otherwise, there were no remarkable differences between the wild type or HM-DKO maps. Also,

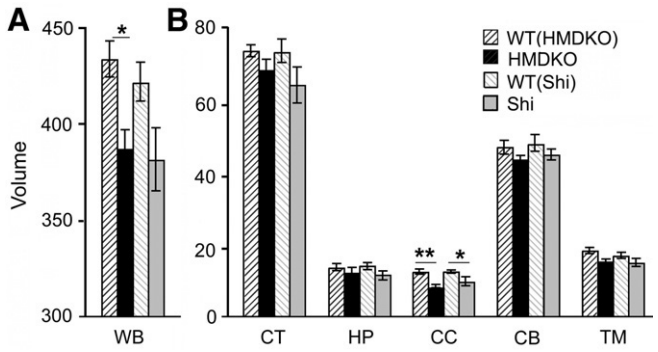

Fig. 1. Volumetric measurements. Whole brain (WB) volume (A) was significantly reduced in the HM-DKO mice (10% reduction, $p<0.01$), but not in Shi mice ($p>0.05$), when compared to their corresponding WT mice. Regional comparisons revealed disproportionately greater loss of volume in the corpus callosum (CC) than in other brain regions (B) in both HM-DKO mice (32% reduction, $p<0.001$) and SH mice (22% reduction, $p<0.05$) when compared to WT controls. [cortex (CT), hippocampus (HP), cerebellum (CB), thalamus (TM), anterior commissure (AC, not shown)].

presented in Table 1 are the means and standard deviations from the ROIs over the corpus callosum. The T2s were consistent with the group estimates (see below) while the standard deviations across the pixels within the ROIs were smallest for the shiverer animal.

Shi mice exhibited increased T2 times in the major WM tracts within subcortical regions such as CC (14% increase), AC ($p<0.0001$), and TM (Fig. 3). By contrast, HM-DKO mice exhibited a modest increase in T2 in the CC (5%), and no significant differences in AC, CT, HP, CB and TM compared to WT(HM-DKO) mice. Because of the smaller sample sizes used in this study, we confirmed the results obtained using parametric statistical analyses of the CC with further non-parametric methods. The Kruskal–Wallis test for T2 data suggested normality ($p=0.071$) but also suggested non-equal variances were likely ($p=0.043$). The analysis of variance indicated a highly significant difference was likely between these groups, so we proceeded to examine differences in the mean T2 of the CC using the Welch's *t*-test, a non-parametric test for distributions with unequal variances. These analyses confirmed that T2 measurements in the CC were statistically different between WT (Shi) and Shi ($p<0.0001$) and WT(HM-DKO) HM-DKO ($p=0.0397$).

In addition, the majority of voxels in the CC exhibited higher T2 values than those in the adjacent cortex, which results in a reversed contrast between WM and gray matter in T2-weighted images for shiverer mice (data not shown). In T2-weighted images, the contrast between the GM and the WM was preserved in the HM-DKO mouse (data not shown). Because we were primarily interested in the effects of alterations in brain myelin upon the T2, we restricted our analysis to tissues within the CC, where a homogeneous tissue sample could be obtained for further morphological analysis.

Table 1
The means and standard deviations (sd) of T2 and se from the ROIs over the corpus callosum (see Fig. 2).

	Standard error (se)		T2 (ms)	
Genotype	Mean	sd	Mean	sd
Shi	$0.38*10^{-4}$	$0.33*10^{-4}$	42.0	2.7
WT(Shi)	$0.74*10^{-4}$	$0.68*10^{-4}$	38.7	3.8
HM-DKO	$0.82*10^{-4}$	$0.57*10^{-4}$	36.9	3.9
WT(HM-DKO)	$1.67*10^{-4}$	$1.8*10^{-4}$	34.3	4.5

Effects of altered NF upon myelin in HM-DKO mice

To investigate the impact of an absence of NF-H and NF-M on cytoskeletal composition, we examined all four of the NF subunits of CNS, namely NF-H, NF-M, NF-L and α-internexin in the CC of HM-DKO mice and their WT controls. As previously seen (Yuan et al., 2006), the HM-DKO mice lacked both NF-H and NF-M (Figs. 4A, D, G, J), as they are not genetically encoded to express these proteins. Interestingly, the total absence of NF-M and NF-H proteins markedly reduced NF-L (Figs. 4A and M) and α-internexin (not shown) to a level that is almost invisible in our Western blot analysis due to *in vivo* proteolytic degradation (Fig. 4A) resulting in the virtual elimination of assembled NFs in axons of HM-DKO mice (Figs. 4A, D, G, J, M). Immunohistochemical detection of MBP in the CC of HM-DKO mice did not reveal substantial differences from the levels seen in WT (HM-DKO) animals (Fig. 4P compared to N). Analysis of the same neurofilament markers in Shi mice (Figs. 4C, F, I, L) did not demonstrate substantial differences from their controls (Figs. 4B, E, H, K). As expected, Shi mice did not demonstrate immunolabeling of MBP (Fig. 4O).

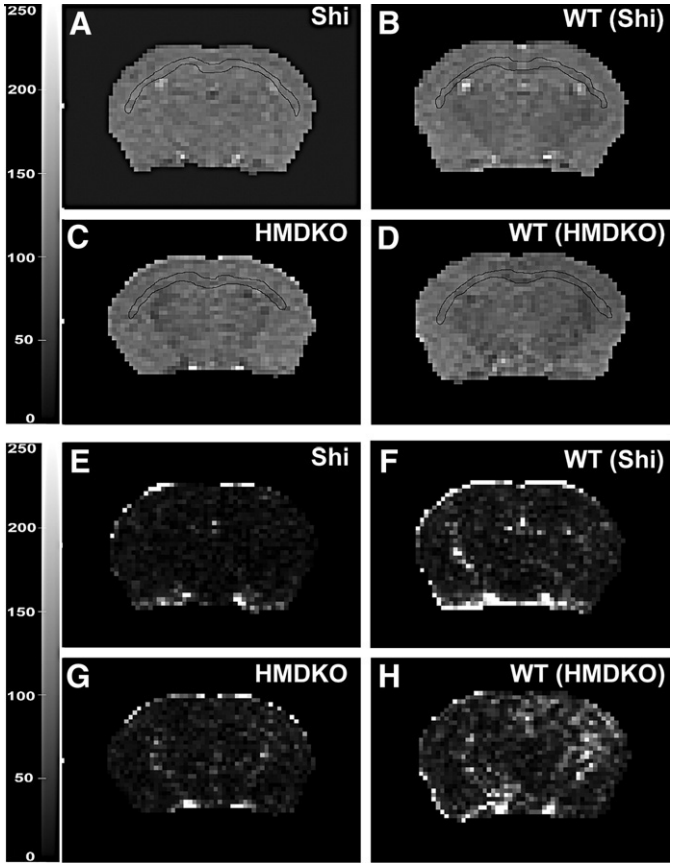

Fig. 2. Examples of representative T2 maps from each of the four genotypes. A—Shi, B—(WT)Shi, C—HM-DKO, D—WT(HM-DKO), region of corpus callosum analyzed is outlined. Corresponding maps of squared error (se) (E, F, G, H). Gray scale: 0–250.

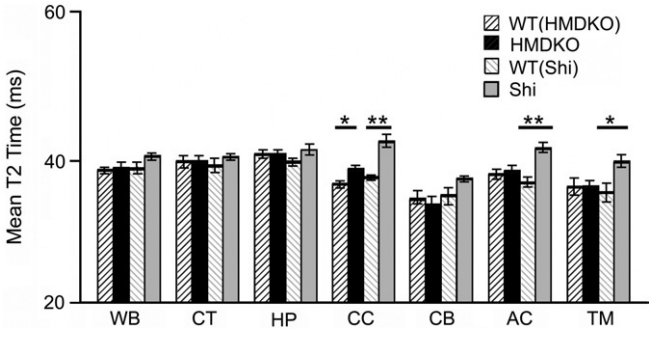

Fig. 3. T2 measurement. Regional representation of T2 data (mean and sd): corpus callosum (CC), cortex (CT), hippocampus (HP), cerebellum (CB), thalamus (TM), anterior commissure (AC). Shi and HM-DKO mice were compared to their corresponding WT controls.

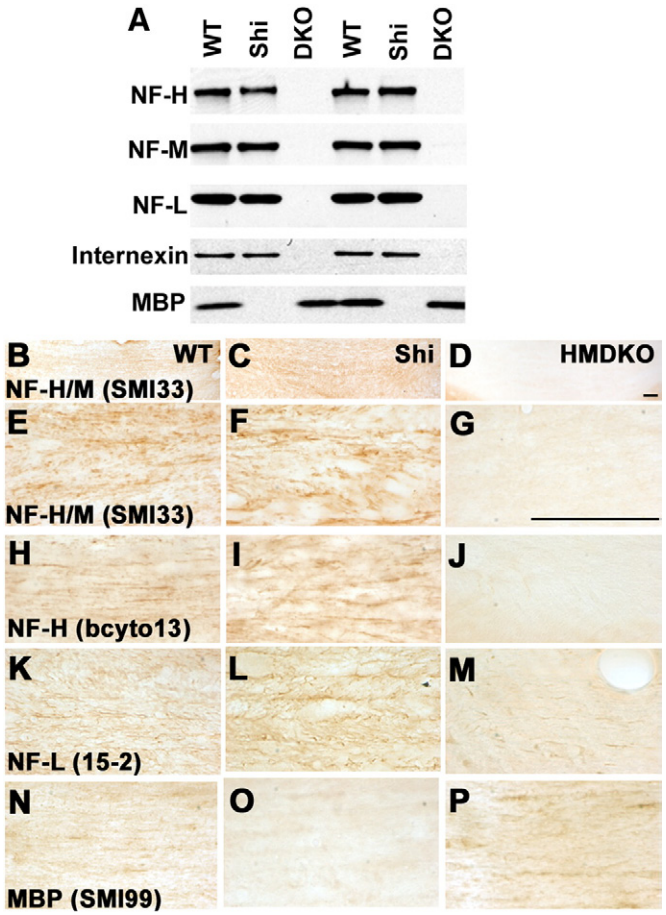

Fig. 4. Immunohistochemistry of the corpus callosum. In two duplicate sets of mice (first 3 vs. second 3 lanes of the gel), western blot analysis (A) reveals that NF-H and NF-M are not expressed in HM-DKO mice and NF-L and α-internexin are below detectable levels. MBP is not expressed in Shi mice. Immunohistochemistry confirms that NF-H and NF-M are not expressed in HM-DKO mice (D, G, J), while in Shi mice (C, F, I), expression levels are comparable to those in WT (B, E, H). NF-L immunolabeling in HM-DKO is greatly reduced (A, M) compared to WT (A, K) and Shi (A, L). Levels of MBP immunoreactivity in WT (N) and HM-DKO (P) are comparable but MBP is absent in Shi mice (O). Scale bar = 50 μm.

Quantitative ultrastructural comparison of myelinated fibers in the corpus callosum of Shi and HM-DKO mice and WT controls

We investigated differences in the microstructure of the CC (see Fig. 4) in both the shiverer and HM-DKO mice as well as their respective WT controls using electron microscopy. Ultrastructural differences are evident in the micrographs of the CC displayed in Figs. 5A–D. Quantification of the cross-sectional areas of myelinated and unmyelinated callosal axons, total area of myelin, and total remaining area (mostly composed of glial processes) is represented in Fig. 5E. The wild type control mice from each group exhibited small but statistically insignificant differences in the percent area contribution to myelin and myelinated axon cross-sectional areas. In HM-DKO mice, neurofilament number in myelinated axons was markedly reduced compared to the number in WT(HM-DKO) mice (Figs. 5B, B1 vs. A, A1). The total areas occupied by myelinated and unmyelinated axons in either WT model were comparable to those measured in HM-DKO mice (S(my) + S(un), Fig. 5E). Total areas of myelin in the WT (HM-DKO), WT (Shi) and HM-DKO mice were comparable (15–18%) (Fig. 5) and contrasted with the near complete absence of myelin in the Shi mouse.

Shi mice exhibited a marked reduction in the number of myelinated axons and an increase in the number of unmyelinated axons (Fig. 5D), which occupied the vast majority of the CC volume. Total axon cross-sectional area in Shi mice was also comparable to the other three mouse lines, but was comprised almost exclusively of unmyelinated axons. In general, the unmyelinated axons in the CC of Shi mice appeared larger than those in WT(Shi) (Figs. 5D vs. C). Myelinated axons were relatively rare in Shi mice, and their myelin sheaths were much thinner than the sheaths of either the WT (Shi), WT(HM-DKO) or HM-DKO mice (data not shown). The total area occupied by glial processes was increased in the Shi mice commensurate with the reduction in myelin, consistent with previous observations of glial proliferation in the Shi brain (Bu et al., 2004).

Discussion

In this study, we have shown that myelin content is minimally affected in HM-DKO mice making them a useful model of primary axonal cytoskeleton disruption. Thus, we have established Shi and HM-DKO mice as contrasting animal models that represent, respectively, a primary dysmyelination and a primary alteration of the intra-axonal compartment secondary to NF loss. Using transverse T2 relaxation time as a pathophysiological index, we have mapped T2 changes *in vivo* in the two genetic mouse models and in their wild type (WT) control animals. Striking differences in the spatial distribution and extent of T2 were observed between these models. By employing immunocytochemical and ultrastructural techniques, we demonstrated that the relaxographic differences between these genetic models can be explained at the molecular and structural levels principally in terms of the alterations in myelin content and overall axonal structure. We also demonstrate substantially larger increases in the T2 of the shiverer mouse than what was observed in the HM-DKO mouse, suggesting a more pronounced effect upon T2 from the myelin deficiency than from neurofilament structure.

In Shi mice, mutation of MBP prevents myelin formation around most CNS axons although oligodendroglia mature and obvious axonal injury and inflammation are absent (Griffiths et al., 1998; Inoue et al., 1981; Privat et al., 1979; Rosenbluth, 1980). At the same time, dysmyelination leads to reduced nerve conduction velocity (Court et al., 2008). Microtubule density in large Shi axons is slightly increased and microtubule stability is decreased (Kirkpatrick et al., 2001), but the latter effect is probably reflective of changes in oligodendroglia (Galiano et al., 2006). In these animals, enhanced proliferation of progenitors to mature oligodendroglia compensates for the loss of myelin, such that in Shi spinal cord, a 2-fold increase in the number of oligodendrocytes has been observed (Bu et al., 2004). This observation likely accounts for the larger total cross-sectional areas of glial processes that we observed in the Shi mouse corpus callosum. The striking T2 changes seen in Shi mice in the CC (the main point of our discussion), may be attributed to several effects. A reduction in myelinated axons likely contributed to increased T2 because water trapped within the myelin folds is short compared to that of water within the axon or outside the myelin/axonal structure. The loss of myelin water was accompanied by a corresponding increase in the cross-sectional area of the intra-axonal water compartment, thus lengthening the T2. This effect is consistent with the longer T2 of the intra-axonal compartment proposed by others (Andrews et al., 2005; Lancaster et al., 2003). In addition, oligodendrocytes, the predominant iron-containing cells in the brain, normally contain transferrin, the iron mobilization protein. In Shi mice, a 1/2 to 2/3 decrease in transferrin protein has been reported in all brain regions examined except for the spinal cord, which could also contribute to the observed increase in T2 (Connor et al., 1993; Ortiz et al., 2004; Portnoy and Stanisz, 2007).

In contrast to Shi mice, HM-DKO mice exhibited only a modest increase of T2 in the CC and relatively minimal changes in other areas when compared to WT (HM-DKO). Dramatic changes in the intra-axonal compartment involving transformation of axoplasm from a predominantly NF-based cytoskeleton to a predominantly

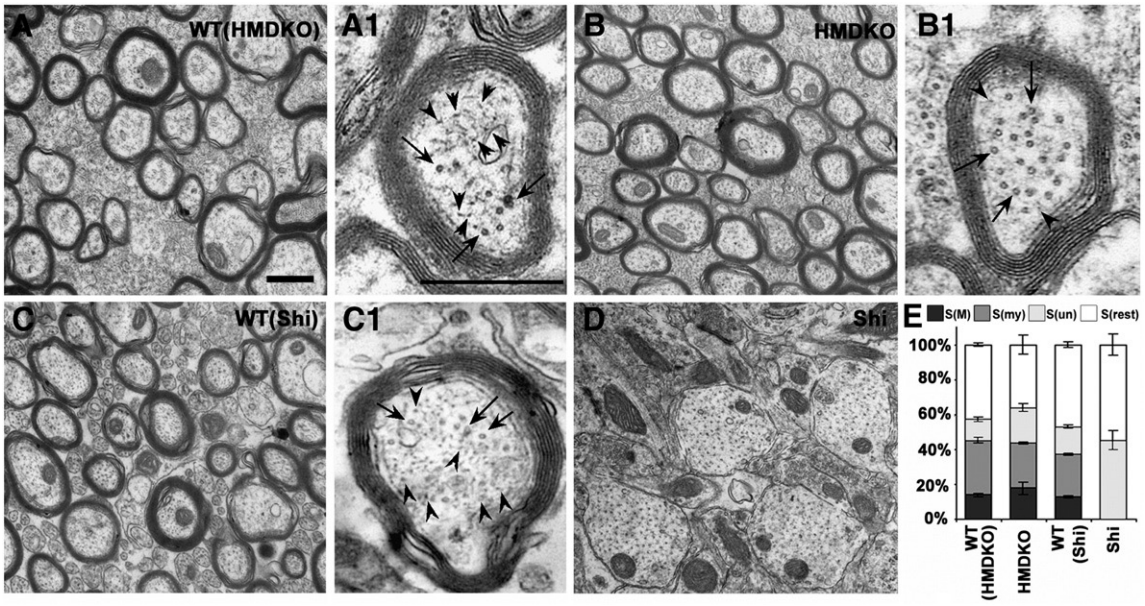

Fig. 5. Quantitative ultrastructure of axons in the corpus callosum. Representative ultrastructural images of the corpus callosum in WT(HM-DKO) (A), HM-DKO (B), WT(Shi) (C) and Shi (D) mice illustrate the fine structure of myelin and axoplasm in low magnification micrographs (panels A–D) and higher power micrographs of representative axons (panels A1–C1). Neurofilaments (arrow heads), but not microtubules (arrows), are markedly reduced in HM-DKO (B1) compared to WT(HM-DKO) (A1) and WT(Shi) (C1). Myelin is nearly uniform in thickness in WT(HM-DKO), WT(Shi) and HM-DKO (panels B, C), but is nearly non-existent in Shi mice (D). In a total of 67 micrographs representing 910–1026 callosal axons from 3 to 4 mice of each genotype (see Materials and methods), the total cross-sectional areas occupied by myelinated—*S*(my), unmyelinated—*S*(un) axons, myelin—*S*(M) and remaining space—*S*(rest) (mainly glial cells and their processes) are quantified. Error bars are standard error of the mean (SE) (panel E). Scale bars = 500 nm.

microtubule-based cytoskeleton (Elder et al., 1999; Jacomy et al., 1999) may have led to the slight net increase in T2 in the CC, although T2 in other brain regions was negligibly altered. We detected minimal differences in the cross-sectional areas of myelin in the HM-DKO mice compared to WT controls consistent with the observations in Shi mice that myelin loss accounts for the large change in T2. Moreover, the finding that the relative space occupied by myelinated and unmyelinated axons was unchanged in HM-DKO animals compared to the WT (HM-DKO) animals minimizes any possibility of a contribution to T2 changes.

T2 relaxometry in the WM is complicated by the heterogeneous environment of water (Beaulieu et al., 1998; Stanisz and Henkelman, 1998) and recent studies have demonstrated the possibility of distinguishing these environments by fitting multiple compartments of T2 relaxation to high-resolution MRI data collected with many echos (Henkelman et al., 2002; Kolind et al., 2008; MacKay et al., 2006; MacKay et al., 2009; Whittall et al., 1997). However, multi-compartmental fitting of exponentially decaying data rarely yield an unambiguous solution (Andrews et al., 2005; Lancaster et al., 2003), especially when the "weight" of one compartment significantly exceeds that of the others. This is likely in the shiverer mouse white matter in which the axoplasmic compartment is the only substantial compartment. In the CC, the remaining unmyelinated axons and oligodendroglia, which are likely to have similar, if not equivalent, T2 relaxation times make up the remaining predominant compartment. Thus, there is essentially one compartment with an intermediate rate constant which we determined to have a T2 of approximately 42 ms. This number is almost exactly that reported in multi-compartmental models of WM for the intermediate rate constant which has been attributed to axoplasmic constituents (Lancaster et al., 2003) and is in agreement with data acquired in optic nerve of the same animal model, utilizing DTI and quantitative magnetization transfer (qMT) approaches (Ou et al., 2009), as well as that of Martin et al., in the Shi mice (Martin et al., 2006). Alternatively, the T2 increase in the Shi mouse might be construed to result from the dramatic loss of lipids in the membranous compartment (lipid bilayer) as well as a reduced brain lipid composition (gangliosides, neutral glycosphingolipids, phospholipids and cholesterol) (Prinetti et al., 2009), associated with the reduced myelin content. Some contribution probably also arises from an associated reduction in intra-axonal iron content (Connor et al., 1993; Ortiz et al., 2004; Portnoy and Stanisz, 2007).

In HM-DKO mice compared to corresponding WT control mice, T2 was only slightly modified despite the complete loss of NF structure. This suggests that the single compartment T2 estimates are less sensitive to axoplasm/axolemma T2 (assuming that indeed, the loss of neurofilament lattice in these animals alters the axolemma T2), than they are to significant changes in myelin content as was observed by us in the shiverer mice. This effect is consistent with, a significantly shorter T2 of water trapped within the myelin folds (as others have noted, Andrews et al., 2005). Interestingly, when we examined the standard deviation across voxels within the CC within individual animals, the variance of the voxel-wise T2 fits was reduced in the test animals when compared to the wild type animals, suggesting better single compartment fits to the data, which would be consistent with reduced compartmentation. On the other hand, the standard deviation of T2 across the animals within each wild type group was smaller than that observed in each of the test groups (WT(HM-DKO): ± 1.1 ms; HM-DKO: ± 1.6 ms; WT(Shi): ± 0.9 ms; and Shi: ± 2.7 ms) but this was likely due to intra-animal variance, rather than the suitability of the single compartment T2 fit.

Regional volumetric comparisons revealed disproportionately greater loss of volume in the CC than in other brain regions in both HM-DKO mice (32%) and Shi mice (22%) when compared to their WT controls. However, there was a 'trend' toward reduced brain volumes between each model and its wild type control for all regions studied. This 'trend' may have contributed to the finding of a reduction in whole brain volume between each animal model and its wild type control group. Since the animals were age matched, and since we did not observe any other factor that may have contributed to this whole brain volume difference, we cannot draw a conclusion regarding the cause of the observation.

We have found that Shi and HM-DKO mice are valuable models for studying the pathological substrate of WM disorders as demonstrated by relaxometry-based MRI. Because MRI relaxometry is typically employed to provide simple, single compartment estimates of water relaxation *in vivo* in an effort to predict or characterize tissue pathology, it is important that we understand the impact of axonal morphology (cellular structure) and composition upon the measures. Clearly, these mouse models permit assessment of the relative contributions of the most critical tissue structures and their consequent effects upon macroscopic MRI measurements. These models, combined with immunohistochemical and EM methodologies, have also demonstrated that simple, single compartment relaxometry is sensitive to substantial ultrastructural changes in WM structure. Sensitivity of these measures to the integrity of the intra-axonal compartment is less prominent. Further study of these animal models, combining ICC and EM methodologies with multi-compartment relaxography assessment of tissue T2 may permit clarification of the role of each of the presumed compartments upon the observed MRI measure, further improving the specificity of MRI relaxometry to WM pathology.

In conclusion, EM morphological assessment of tissue compartmentalization, combined with DTI of myelin pathology, multi-compartmental T2 MRI and possibly magnetization transfer may someday permit distinction between disorders involving myelination and those involving axonal loss. Human studies at higher magnetic fields (3 T and above) and improved methods for parameter quantification may eventually center on these measurements the specificity available in small animals and higher field strengths (Choi et al., 2009; Madhavarao et al., 2005; Ratai et al., 2008). Development of measurements sensitive to the substructure and composition of white matter will enhance our ability to characterize the morphology and state of white matter pathology in progressive diseases such as schizophrenia, MS and Alzheimer's disease.

Acknowledgments

We thank Dr. David Guilfoyle for development of the quantitative MRI protocol and Nicole Piorkowski for assistance with manuscript preparation. This work was supported by Grant 5R01AG005604 (R.A.N.) from the National Institutes on Aging.

References

Andrews, T., Lancaster, J.L., Dodd, S.J., Contreras-Sesvold, C., Fox, P.T., 2005. Testing the three-pool white matter model adapted for use with T2 relaxometry. Magn. Reson. Med. 54, 449–454.

Beaulieu, C., Fenrich, F.R., Allen, P.S., 1998. Multicomponent water proton transverse relaxation and T2-discriminated water diffusion in myelinated and nonmyelinated nerve. Magn. Reson. Imaging 16, 1201–1210.

Brant-Zawadzki, M., Fein, G., Van Dyke, C., Kiernan, R., Davenport, L., de Groot, J., 1985. MR imaging of the aging brain: patchy white-matter lesions and dementia. AJNR Am. J. Neuroradiol. 6, 675–682.

Bu, J., Banki, A., Wu, Q., Nishiyama, A., 2004. Increased NG2(+) glial cell proliferation and oligodendrocyte generation in the hypomyelinating mutant shiverer. Glia 48, 51–63.

Chen, Y., Dyakin, V.V., Branch, C.A., Ardekani, B., Yang, D., Guilfoyle, D.N., Peterson, J., Peterhoff, C., Ginsberg, S.D., Cataldo, A.M., Nixon, R.A., 2009. In vivo MRI identifies cholinergic circuitry deficits in a Down syndrome model. Neurobiol. Aging 30, 1453–1465.

Cheung, V., Cheung, C., McAlonan, G.M., Deng, Y., Wong, J.G., Yip, L., Tai, K.S., Khong, P.L., Sham, P., Chua, S.E., 2008. A diffusion tensor imaging study of structural dysconnectivity in never-medicated, first-episode schizophrenia. Psychol. Med. 38, 877–885.

Choi, C., Dimitrov, I., Douglas, D., Zhao, C., Hawesa, H., Ghose, S., Tamminga, C.A., 2009. In vivo detection of serine in the human brain by proton magnetic resonance spectroscopy (1H-MRS) at 7 Tesla. Magn. Reson. Med. 62, 1042–1046.

Connor, J.R., Roskams, A.J., Menzies, S.L., Williams, M.E., 1993. Transferrin in the central nervous system of the shiverer mouse myelin mutant. J. Neurosci. Res. 36, 501–507.

Court, F.A., Brophy, P.J., Ribchester, R.R., 2008. Remodeling of motor nerve terminals in demyelinating axons of periaxin-null mice. Glia 56, 471–479.

Degaonkar, M.N., Raghunathan, P., Jayasundar, R., Jagannathan, N.R., 2005. Determination of relaxation characteristics during preacute stage of lysophosphatidyl choline-induced demyelinating lesion in rat brain: an animal model of multiple sclerosis. Magn. Reson. Imaging 23, 69–73.

Elder, G.A., Friedrich Jr., V.L., Pereira, D., Tu, P.H., Zhang, B., Lee, V.M., Lazzarini, R.A., 1999. Mice with disrupted midsized and heavy neurofilament genes lack axonal neurofilaments but have unaltered numbers of axonal microtubules. J. Neurosci. Res. 57, 23–32.

Falangola, M.F., Ardekani, B.A., Lee, S.P., Babb, J.S., Bogart, A., Dyakin, V.V., Nixon, R., Duff, K., Helpern, J.A., 2005. Application of a non-linear image registration algorithm to quantitative analysis of T2 relaxation time in transgenic mouse models of AD pathology. J. Neurosci. Methods 144, 91–97.

Falangola, M.F., Dyakin, V.V., Lee, S.P., Bogart, A., Babb, J.S., Duff, K., Nixon, R., Helpern, J.A., Helpern, J.A., 2007. Quantitative MRI reveals aging-associated T(2) changes in mouse models of Alzheimer's disease. NMR Biomed. 20, 343–351.

Figiel, G.S., Krishnan, K.R., Rao, V.P., Doraiswamy, M., Ellinwood Jr., E.H., Nemeroff, C.B., Evans, D., Boyko, O., 1991. Subcortical hyperintensities on brain magnetic resonance imaging: a comparison of normal and bipolar subjects. J. Neuropsychiatry Clin. Neurosci. 3, 18–22.

Ford, C.C., Ceckler, T.L., Karp, J., Herndon, R.M., 1990. Magnetic resonance imaging of experimental demyelinating lesions. Magn. Reson. Med. 14, 461–481.

Franklin, K.B.J., Paxinos, G., 1997. The Mouse Brain in Stereotaxic Coordinates. Academic Press, London, UK.

Galiano, M.R., Andrieux, A., Deloulme, J.C., Bosc, C., Schweitzer, A., Job, D., Hallak, M.E., 2006. Myelin basic protein functions as a microtubule stabilizing protein in differentiated oligodendrocytes. J. Neurosci. Res. 84, 534–541.

Giacomini, P.S., Levesque, I.R., Ribeiro, L., Narayanan, S., Francis, S.J., Pike, G.B., Arnold, D.L., 2009. Measuring demyelination and remyelination in acute multiple sclerosis lesion voxels. Arch. Neurol. 66, 375–381.

Griffiths, I., Klugmann, M., Anderson, T., Yool, D., Thomson, C., Schwab, M.H., Schneider, A., Zimmermann, F., McCulloch, M., Nadon, N., Nave, K.A., 1998. Axonal swellings and degeneration in mice lacking the major proteolipid of myelin. Science 280, 1610–1613.

Guilfoyle, D.N., Dyakin, V.V., O'Shea, J., Pell, G.S., Helpern, J.A., 2003. Quantitative measurements of proton spin-lattice (T1) and spin-spin (T2) relaxation times in the mouse brain at 7.0 T. Magn. Reson. Med. 49, 576–580.

Henkelman, R.M., Stanisz, G.J., Menezes, N., Burstein, D., 2002. Can MTR be used to assess cartilage in the presence of Gd-DTPA2−? Magn. Reson. Med. 48, 1081–1084.

Inoue, Y., Nakamura, R., Mikoshiba, K., Tsukada, Y., 1981. Fine structure of the central myelin sheath in the myelin deficient mutant Shiverer mouse, with special reference to the pattern of myelin formation by oligodendroglia. Brain Res. 219, 85–94.

Jacomy, H., Zhu, Q., Couillard-Despres, S., Beaulieu, J.M., Julien, J.P., 1999. Disruption of type IV intermediate filament network in mice lacking the neurofilament medium and heavy subunits. J. Neurochem. 73, 972–984.

Kaye, E.M., 2001. Update on genetic disorders affecting white matter. Pediatr. Neurol. 24, 11–24.

Kerschensteiner, M., Bareyre, F.M., Buddeberg, B.S., Merkler, D., Stadelmann, C., Bruck, W., Misgeld, T., Schwab, M.E., 2004. Remodeling of axonal connections contributes to recovery in an animal model of multiple sclerosis. J. Exp. Med. 200, 1027–1038.

Kirkpatrick, L.L., Witt, A.S., Payne, H.R., Shine, H.D., Brady, S.T., 2001. Changes in microtubule stability and density in myelin-deficient shiverer mouse CNS axons. J. Neurosci. 21, 2288–2297.

Kolind, S.H., Laule, C., Vavasour, I.M., Li, D.K., Traboulsee, A.L., Madler, B., Moore, G.R., Mackay, A.L., 2008. Complementary information from multi-exponential T2 relaxation and diffusion tensor imaging reveals differences between multiple sclerosis lesions. Neuroimage 40, 77–85.

Lancaster, J.L., Andrews, T., Hardies, L.J., Dodd, S., Fox, P.T., 2003. Three-pool model of white matter. J. Magn. Reson. Imaging 17, 1–10.

Laule, C., Kozlowski, P., Leung, E., Li, D.K., Mackay, A.L., Moore, G.R., 2008. Myelin water imaging of multiple sclerosis at 7 T: correlations with histopathology. Neuroimage 40, 1575–1580.

MacKay, A., Laule, C., Vavasour, I., Bjarnason, T., Kolind, S., Madler, B., 2006. Insights into brain microstructure from the T2 distribution. Magn. Reson. Imaging 24, 515–525.

MacKay, A.L., Vavasour, I.M., Rauscher, A., Kolind, S.H., Madler, B., Moore, G.R., Traboulsee, A.L., Li, D.K., Laule, C., 2009. MR relaxation in multiple sclerosis. Neuroimaging Clin. N. Am. 19, 1–26.

Madhavarao, C.N., Arun, P., Moffett, J.R., Szucs, S., Surendran, S., Matalon, R., Garbern, J., Hristova, D., Johnson, A., Jiang, W., Namboodiri, M.A., 2005. Defective N-acetylaspartate catabolism reduces brain acetate levels and myelin lipid synthesis in Canavan's disease. Proc. Natl. Acad. Sci. U. S. A. 102, 5221–5226.

Martin, M., Hiltner, T.D., Wood, J.C., Fraser, S.E., Jacobs, R.E., Readhead, C., 2006. Myelin deficiencies visualized in vivo: visually evoked potentials and T2-weighted magnetic resonance images of shiverer mutant and wild-type mice. J. Neurosci. Res. 84, 1716–1726.

McArdle, C.B., Richardson, C.J., Nicholas, D.A., Mirfakhraee, M., Hayden, C.K., Amparo, E.G., 1987. Developmental features of the neonatal brain: MR imaging. Part I. Gray-white matter differentiation and myelination. Radiology 162, 223–229.

McCreary, C.R., Bjarnason, T.A., Skihar, V., Mitchell, J.R., Yong, V.W., Dunn, J.F., 2009. Multiexponential T2 and magnetization transfer MRI of demyelination and remyelination in murine spinal cord. Neuroimage 45, 1173–1182.

Ortiz, E., Pasquini, J.M., Thompson, K., Felt, B., Butkus, G., Beard, J., Connor, J.R., 2004. Effect of manipulation of iron storage, transport, or availability on myelin composition and brain iron content in three different animal models. J. Neurosci. Res. 77, 681–689.

Ou, X., Sun, S.W., Liang, H.F., Song, S.K., Gochberg, D.F., 2009. Quantitative magnetization transfer measured pool-size ratio reflects optic nerve myelin content in ex vivo mice. Magn. Reson. Med. 61, 364–371.

Pascual-Lozano, A.M., Martinez-Bisbal, M.C., Bosca-Blasco, I., Valero-Merino, C., Coret-Ferrer, F., Marti-Bonmati, L., Martinez-Granados, B., Celda, B., Casanova-Estruch, B., 2007. Total brain T2-hyperintense lesion-volume and the axonal damage in the normal-appearing white matter of brainstem in early lapsing-remitting multiple sclerosis. Rev. Neurol. 45, 468–473.

Portnoy, S., Stanisz, G.J., 2007. Modeling pulsed magnetization transfer. Magn. Reson. Med. 58, 144–155.
Prinetti, A., Rocchetta, F., Costantino, E., Frattini, A., Caldana, E., Rucci, F., Bettiga, A., Poliani, P.L., Chigorno, V., Sonnino, S., 2009. Brain lipid composition in grey-lethal mutant mouse characterized by severe malignant osteopetrosis. Glycoconj. J. 26, 623–633.
Privat, A., Jacque, C., Bourre, J.M., Dupouey, P., Baumann, N., 1979. Absence of the major dense line in myelin of the mutant mouse "shiverer". Neurosci. Lett. 12, 107–112.
Rao, M.V., Mohan, P.S., Peterhoff, C.M., Yang, D.S., Schmidt, S.D., Stavrides, P.H., Campbell, J., Chen, Y., Jiang, Y., Paskevich, P.A., Cataldo, A.M., Haroutunian, V., Nixon, R.A., 2008. Marked calpastatin (CAST) depletion in Alzheimer's disease accelerates cytoskeleton disruption and neurodegeneration: neuroprotection by CAST overexpression. J. Neurosci. 28, 12241–12254.
Ratai, E., Kok, T., Wiggins, C., Wiggins, G., Grant, E., Gagoski, B., O'Neill, G., Adalsteinsson, E., Eichler, F., 2008. Seven-Tesla proton magnetic resonance spectroscopic imaging in adult X-linked adrenoleukodystrophy. Arch. Neurol. 65, 1488–1494.
Rosenbluth, J., 1980. Central myelin in the mouse mutant shiverer. J. Comp. Neurol. 194, 639–648.
Seiwa, C., Kojima-Aikawa, K., Matsumoto, I., Asou, H., 2002. CNS myelinogenesis in vitro: myelin basic protein deficient shiverer oligodendrocytes. J. Neurosci. Res. 69, 305–317.
Shen, X.Y., Billings-Gagliardi, S., Sidman, R.L., Wolf, M.K., 1985. Myelin deficient (shimld) mutant allele: morphological comparison with shiverer (shi) allele on a B6C3 mouse stock. Brain Res. 360, 235–247.
Song, S.K., Sun, S.W., Ramsbottom, M.J., Chang, C., Russell, J., Cross, A.H., 2002. Dysmyelination revealed through MRI as increased radial (but unchanged axial) diffusion of water. Neuroimage 17, 1429–1436.
Stanisz, G.J., Henkelman, R.M., 1998. Diffusional anisotropy of T2 components in bovine optic nerve. Magn. Reson. Med. 40, 405–410.
Trapp, B.D., Ransohoff, R., Rudick, R., 1999. Axonal pathology in multiple sclerosis: relationship to neurologic disability. Curr. Opin. Neurol. 12, 295–302.
Valk, J., Barkhof, F., 2005. Multiple sclerosis. In: van der Knapp, M.S., Valk, J. (Eds.), Magnetic Resonance of Myelination and Myelin Disorders. Springer, New York, pp. 566–603.
Veeranna, Kaji, T., Boland, B., Odrljin, T., Mohan, P., Basavarajappa, B.S., Peterhoff, C., Cataldo, A., Rudnicki, A., Amin, N., Li, B.S., Pant, H.C., Hungund, B.L., Arancio, O., Nixon, R.A., 2004. Calpain mediates calcium-induced activation of the erk1,2 MAPK pathway and cytoskeletal phosphorylation in neurons: relevance to Alzheimer's disease. Am. J. Pathol. 165, 795–805.
Whittall, K.P., MacKay, A.L., Graeb, D.A., Nugent, R.A., Li, D.K., Paty, D.W., 1997. In vivo measurement of T2 distributions and water contents in normal human brain. Magn. Reson. Med. 37, 34–43.
Yuan, A., Rao, M.V., Sasaki, T., Chen, Y., Kumar, A., Veeranna Liem, R.K., Eyer, J., Peterson, A.C., Julien, J.P., Nixon, R.A., 2006. Alpha-internexin is structurally and functionally associated with the neurofilament triplet proteins in the mature CNS. J. Neurosci. 26, 10006–10019.
Yuan, W., Holland, S.K., Schmithorst, V.J., Walz, N.C., Cecil, K.M., Jones, B.V., Karunanayaka, P., Michaud, L., Wade, S.L., 2007. Diffusion tensor MR imaging reveals persistent white matter alteration after traumatic brain injury experienced during early childhood. AJNR Am. J. Neuroradiol. 28, 1919–1925.
Zaaraoui, W., Deloire, M., Merle, M., Girard, C., Raffard, G., Biran, M., Inglese, M., Petry, K. G., Gonen, O., Brochet, B., Franconi, J.M., Dousset, V., 2008. Monitoring demyelination and remyelination by magnetization transfer imaging in the mouse brain at 9.4 T. MAGMA 21, 357–362.